# Generation of polarization-insensitive perfect vortices by dielectric metasurfaces with diverging or converging axicon phases

Zhe Shen[1,*], Longyin Teng[1], Zhiyuan Xiang[1], Le Li[1], Yunjie Rui[1], and Yaochun Shen[2]

[1]*School of Electronic and Optical Engineering, Nanjing University of Science and Technology, Nanjing 210094, China*
[2]*Department of Electrical Engineering & Electronics, University of Liverpool, Liverpool L69 3GJ, UK*
**shenzhe@njust.edu.cn*

**Abstract**

Perfect vortex (PV) is a special light field with constant annular light intensity distribution while carrying orbital angular momentum. It has been widely used in the fields of optical communications and particle manipulation. However, conventional methods to produce PVs require a series of complex components, which limit their practical use in miniaturization. In this paper, we designed PV generators based on highly efficient polarization-insensitive dielectric metasurfaces. Simulation results showed that our designs could generate PVs with arbitrarily polarized incident Gaussian beams. By adjusting the focal length of the lens and the half fan angle of the axicon, ring-shaped focal spots with different radii could be obtained in the propagation space, rendering the system more flexible. Moreover, by superimposing the phase functions of the four PVs with different ring radii , the simulation results demonstrated the generation of coaxial PVs. Meanwhile, the multi-channel PVs were achieved by introducing the linear displacement factors. By employing polarization-insensitive dielectric metasurfaces, we believe that this method of PV generation will stimulate further applications in fields such as optical communications, particle trapping and manipulation.

**Keywords:** Polarization-insensitive metasurfaces; Perfect Vortex beam; Beam shaping.

## 1. Introduction

Optical vortex (OV) is a light field with a spiral wavefront, which carries orbital angular momentum (OAM) and shaped like a ring at the transverse plane. Since the OV was proposed by Allen *et al* [1] in 1992, it has become a research hotspot in emerging fields in optics such as optical trapping [2-4] and optical communications [5, 6]. However, the light field profile of the OV will increase significantly with the increase of the topological charge (TC) it carries. As a result, it is difficult to use OVs with large TCs in some practical applications such as coupling multi-OAMs in a single fiber [7, 8]. In order to solve this problem, perfect vortex (PV) was theoretically proposed and produced in laboratory [9]. The radius of the ring-shaped focal spot is almost fixed as the TCs change. This unique property has also propelled PV to be applied in optical communications [10, 11], particle manipulation [12, 13], and plasmonic structured illumination imaging [14].

Theoretically, PV was produced from the Fourier transform of the Bessel-Gaussian (BG) beam [15], which can be achieved by combining an axicon with the vortex phase obtained from a spatial light modulator (SLM) [12]. However, these core devices used to generate PVs are relatively bulky and complicated, which increases the complexity and decreases the flexibility of the whole optical system. Recently, owing to flexible regulation of the amplitude and phase of the light field, metasurfaces based on sub-wavelength-sized structures have been widely applied in optical systems to achieve miniaturization, high integration, and high-performance applications [16-19]. Due to their unique flexibility, metasurfaces have been widely applied in

the generation of Bessel beams [20-23] and OVs [24-27], which provides a good approach for reducing the complexity of optical systems and brings about new possibilities for the PV generation.

In the early exploration of applying metasurfaces to the PV generation, Liu *et al* [28] firstly produced PVs by replacing the bulky refractive devices with three parts of Pancharatnam-Berry (PB) phase [29-32] elements, which significantly reduced the thickness of the whole system but still left a lot of room to improve the integration. Zhang *et al* [33] took a monolithic plasmonic metasurface based on PB phase to produce PVs and array PVs (multi-channel PVs) with a wide operating band and high flexibility to adjust parameters of the PVs, but the transmission efficiency of plasmonic metasurfaces was relatively low. Recently, with high-contrast dielectric materials [34-36], many researchers used dielectric PB metasurfaces [37,38,46] and successfully produced PVs with their own characteristics. Moreover, by combining geometric and propagation phases, special spin-multiplexed metasurfaces were designed and fabricated, which achieved broadband generation of perfect Poincaré beam [47], a unique superposition of two PVs with different polarization. The dielectric metasurfaces can achieve phase control without ohmic losses, and thus have higher transmission efficiency. However, there is always a limit to the polarization state of the incident light when using PB phase metasurfaces. Polarization-insensitive metasurfaces [39,40], instead, shave similar uses but with fewer restriction of light sources, which have almost uniform responses to incident light in different polarization directions. By using polarization-insensitive metasurfaces, PV-generating devices suitable for general light sources can be generated.

In order to solve the above issues, we designed nano-post units based on dielectric materials to form a polarization-insensitive metasurface. Simulation results showed that, by combining phases of a converging or diverging axicon, a spiral phase plate, and the Fourier transform lens, PVs could be generated by using only a single metasurface and we analyzed the regulation effects of the focal length of the lens and the half fan angle of the axicon. Based on the high flexibility of metasurfaces, we extended the applicable range of the half fan angle in the axicon phase from traditional converging to diverging. Then, to explore further applications of PVs, we investigated two different approaches to generate multiple PVs with monolithic metasurfaces, that is, by superimposing the phase functions of the four PVs with different ring radii to generate the coaxial PVs and introducing the linear displacement factors to achieve the multi-channel PVs. Our work may help PVs develop applications in fields such as optical communications and particle manipulation.

## 2. Method and theory

### *2.1. The metasurface design*

As shown in Figs. 1(a) and (b), the metasurface is composed of cylindrical $TiO_2$ nano-posts placed on $SiO_2$ substrate, in which the phase regulation of the structure is dominated by the waveguide effect [26]. The incident light illuminates on the metasurface from the bottom and generates a ring-shaped focal spot in the designed focal plane. The substrate period of single unit cell is set to $P$ = 325 nm and the height of the $TiO_2$ nano-posts is set as $H$ = 600 nm. By varying the radius of the nano-post, the whole $2\pi$ phase shift can be achieved. We selected the plane wave with a wavelength of $\lambda$ = 532 nm as the incident light source for the simulation of single unit cell and the refractive index of $TiO_2$ at this wavelength is 2.42. Under these conditions, the influence of the radius R of a single structure on incident light is calculated. Here, the finite difference time domain (FDTD) method was used to calculate the relationship between the transmittance and the phase shift characteristics of $TiO_2$ nano-posts with different radii, as shown in Fig. 1(c). Within the scope of $0\sim2\pi$ phase shifts, the transmittance of incident light passing through nano-posts with different radii can be kept above 80%. To verify the polarization insensitivity, we separately calculated the phase regulation of single unit cell under *x*-polarized, *y*-polarized, left-handed circularly polarized, and right-handed circularly polarized incident beams. As shown in Fig. 1(d), almost consistent characteristics of phase shifts can be obtained under differently polarized incident beams, which demonstrates that the PV can be generated using monochromatic light beams of different polarization states.

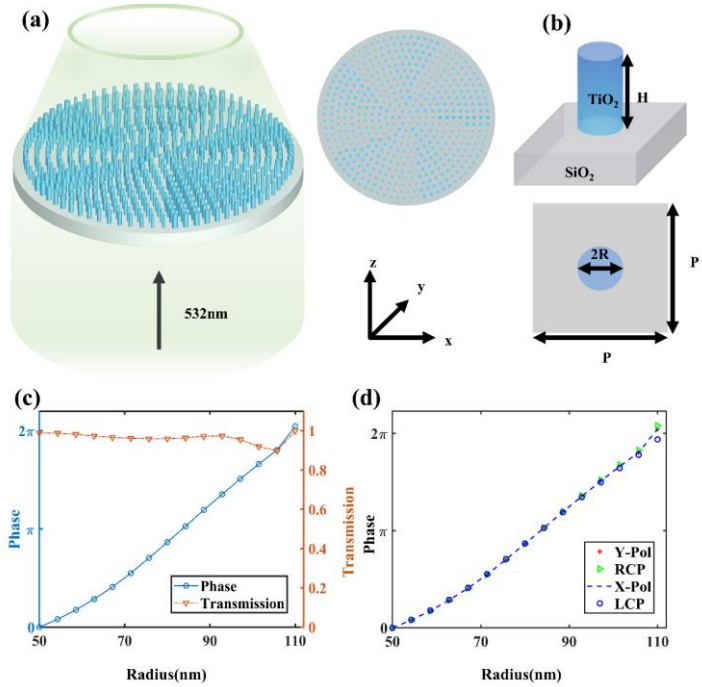


Fig. 1(a) Schematic diagram of the metasurface for generating PV and (b) the unit cell. (c) Curves of transmittance and phase shift of the unit of nanostructure; (d) Curves of the phase shift of the unit of nanostructure under x-polarized, y-polarized, left-handed circularly polarized, and right-handed circularly polarized incident beams, respectively.

### *2.2. The generation method of PV*

By deriving the Fourier transformation of the ideal Bessel beam $E_B$, one can generate an ideal PV beam defined by the Dirac function [9], which can be expressed as Eq. (2).

$$E_B(r,\theta) = J_l(k_r r)\cdot \exp(il\theta + ik_z z), \tag{1}$$

$$E(r,\theta) = \delta(r - r_0)\cdot \exp(il\theta), \tag{2}$$

where $(r,\theta)$ are the polar coordinates, $k = \sqrt{k_r^{\,2} + k_z^{\,2}}$ is the wave vector, which can be decomposed into ($k_r$, $k_z$), the radial and longitudinal wave vectors, and $J_l$ is the $l$th order Bessel function of the first kind. The ideal PV beam will form a ring-shaped focal spot in space, with the value of ring radius $r_0 = k_r \cdot f/k$ and $l$ the topological charge carried. While the ideal Bessel beam carries an infinite amount of energy and cannot be created experimentally, by illuminating the axicons with Gaussian incidences, one can produce a Bessel–Gauss beam $E_{BG}$ with the beam waist $\omega_g$ as an alternative to the ideal one. Again, by deriving the Fourier transformation of the Bessel–Gauss beam [15], the approximation of ideal PV can be expressed as Eq. (4).

$$E_{BG}(r,\theta) = J_l(k_r r)\cdot \exp(il\theta)\cdot \exp\left(-\frac{r^2}{\omega_g^{\,2}}\right), \tag{3}$$

$$E(r,\theta) = i^{l-1} \cdot \frac{\omega_g}{\omega_0} \cdot \exp(il\theta) \cdot \exp\left(-\frac{r^2 + r_0^2}{\omega_0^2}\right) \cdot I_l\left(\frac{2rr_0}{\omega_0^2}\right), \tag{4}$$

where $I_l$ is the $l$th order modified Bessel function of the first kind with the Gaussian beam waist in the focal plane $\omega_0 = 2f / k\omega_g$ . Due to the introduction of the axicon [12], the ring radius can be expressed as $r_0 = k_r \cdot f/k \approx f \cdot \sin(\beta)$ , which means that $r_0$ can be modulated by the half fan angle of the axicon $\beta$ and the focal length of the lens $f$.

The traditional method to generate PVs requires three pivotal components: an axicon, a spiral phase plate, and a Fourier transform lens. In order to replace all three refractive elements involved in the conventional system, by superimposing the phases of these three components, we can obtain the phase function to generate PVs as follows:

$$\varphi_{\mathrm{PV}}(x,y) = \varphi_{\mathrm{axicon}}(x,y) + \varphi_{\mathrm{spiral}}(x,y) + \varphi_{\mathrm{lens}}(x,y), \tag{5}$$

$$\varphi_{\mathrm{axicon}}(x,y) = \frac{2\pi\sqrt{x^2+y^2} \cdot \sin(\beta)}{\lambda}, \tag{6}$$

$$\varphi_{\mathrm{spiral}}(x,y) = m \cdot \arctan\left(\frac{y}{x}\right), \tag{7}$$

$$\varphi_{\mathrm{lens}}(x,y) = \frac{2\pi\left(f - \sqrt{f^2+x^2+y^2}\right)}{\lambda}, \tag{8}$$

where ($x$, $y$) is the Cartesian coordinate established at the center of the upper surface of the metasurfaces, $\lambda$ is the wavelength of the light source, and $\beta$ is the half fan angle of the axicon. Eq. (6) corresponds to diverging or converging axicon phase when $\beta$ is greater than or less than 0, respectively. The $m$ is the TCs and $f$ is the focal length of the lens. In order to generate PV through a monolithic metasurface, we determined the radius and configuration of each nano-post based on the phase equation described in Eq. (5) and the radius-phase curve of the unit cell in Fig. 1(c). Usually, converging axicon is adopted in PV generation, in which the negative half fan angle $\beta$ is chosen, as shown in Fig. 2(a). If $\beta$ is positive, Eq. (5) will appear as a diverging axicon, as shown in Fig. 2(b). The difference between the two kinds of axicons is that their phases have opposite radial phase gradients. In our design, we used both positive and negative $\beta$, that is, using the diverging axicon and converging axicon phase to generate PV. The converging axicon and the diverging axicon are basically a pair of complementary optical elements, and both can achieve a ring-shaped focal pattern [41]. These two kinds of axicons can transform the incidences into real and virtual Bessel beams, respectively [42, 48], and both of their regulation effects on the incident light can be expressed by Eq. (6). When the phase of the axicon is loaded into the metasurface, the symbols of the half fan angle $\beta$ in Eq. (6) can be used to represent the two types of axicons respectively, which again reflects the flexibility of metasurfaces compared to traditional refractive optical elements.

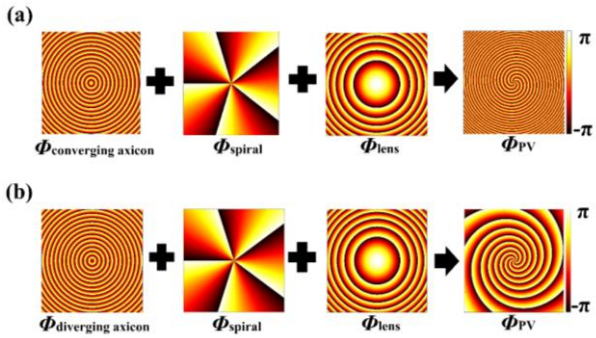


Fig. 2 Taking the PV of $m$ = 5, the Schematic diagram of the beam propagation process and the phase synthesis diagram of the PV generated by (a) converging axicon and (b) diverging axicon.

## 3. Results and discussion

### *3.1. Single PV*

To prove that the metasurface with the converging axicon phase we designed can generate a single PV, we firstly simulated the metasurface through the FDTD method as shown in Fig. 3, and the radius of the metasurface was set as $R$ = 25 μm. In all subsequent simulations, we used a right-handed Gaussian beam as the incident light with the wavelength and beam waist radius set as 532 nm and 2$R$, respectively. Fig. 3(a) shows the phase distributions on the upper surface of the metasurface, and it can be observed that the spiral phase fringes correspond to the preset TCs. According to the obtained light intensity distributions in Fig. 3(b) and the phase distributions in Fig. 3(c), we calculated the ring radii. Here, we chose the distance from the coordinates corresponding to the maximum light intensity at $y$ = 0 μm to the center of the focal plane as the radius of PV. The ring radii of these three PVs in the focal plane were $r_1$ = 11.15 μm ($m$ = 1), $r_2$ = 12.71 μm ($m$ = 5), and $r_3$ = 14.18 μm ($m$ = 10). The radii of the three ring-shaped focal spots were almost unchanged with the growing TCs, which proved that the PV was successfully generated with the preset parameters. The focusing efficiency of the PV generator is defined as the ratio of the transmitted power passing through the ring-shaped pattern whose radius is three times the full width at half-maximum (FWHM) [46]. With the parameters above, the efficiencies of the metasurface generators are 52.08% ($m$ = 1), 58.92% ($m$ = 5), and 54.72% ($m$ = 10). Then we changed the axicon phase into diverging one. Fig. 4(a) shows the phase distributions on the upper surface of the metasurface, and it can be observed that the spiral phase fringes correspond to the preset TCs $m$. As shown in Fig. 4(b), the radii of the three ring-shaped focal spots carrying different TCs were almost the same, with $r_1$ = 14.88 μm ($m$ = 1), $r_2$ = 14.92 μm ($m$ = 5), and $r_3$ = 15.12 μm ($m$ = 10). According to Fig. 4(c), it can be observed that phase fringes corresponding to designed parameters $m$ are generated in the focal plane, corresponding to the ring-shaped focal spots. As the TCs grew, there were only small increases in the ring radius, which means that PVs using diverging axicon phase were successfully generated. And here, the PV generators have the conversion efficiency up to 67.69% ($m$ = 1), 66.14% ($m$ = 5), and 62.27% ($m$ = 10).

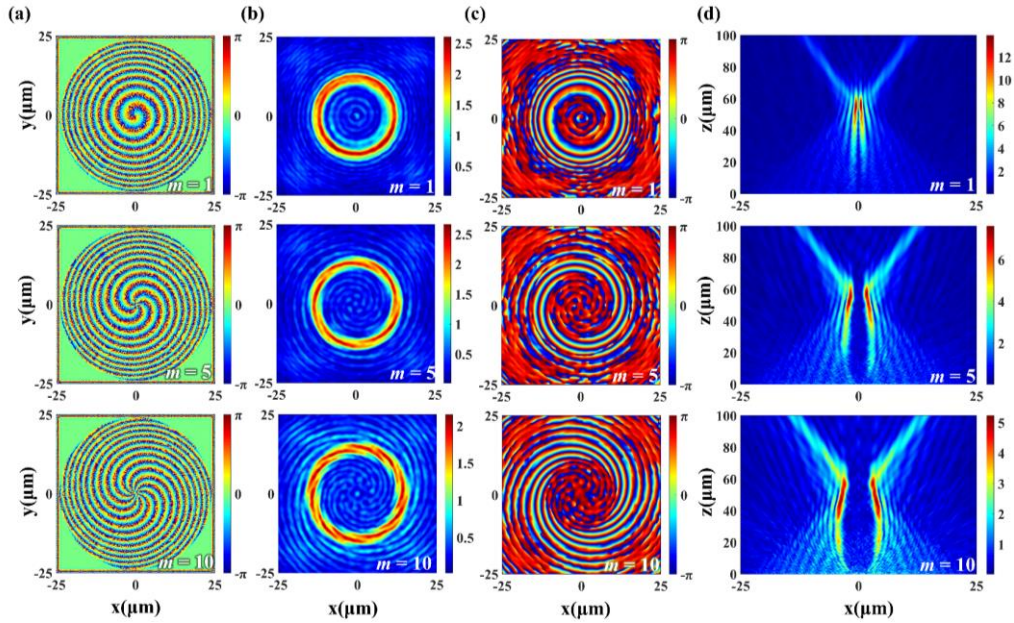


Fig. 3 In the case of axial cone phase convergence, the parameters of the metasurface are $f$ = 100 μm, $\beta$ = -5 °, $m$ = 1,5, and 10. (a) The phase distribution on the upper surface of the metasurfaces is obtained. (b) The intensity distribution in the focal plane $z$ = 100 μm. (c) The phase distribution in the focal plane. (d) The intensity distribution on the z-transmission plane.

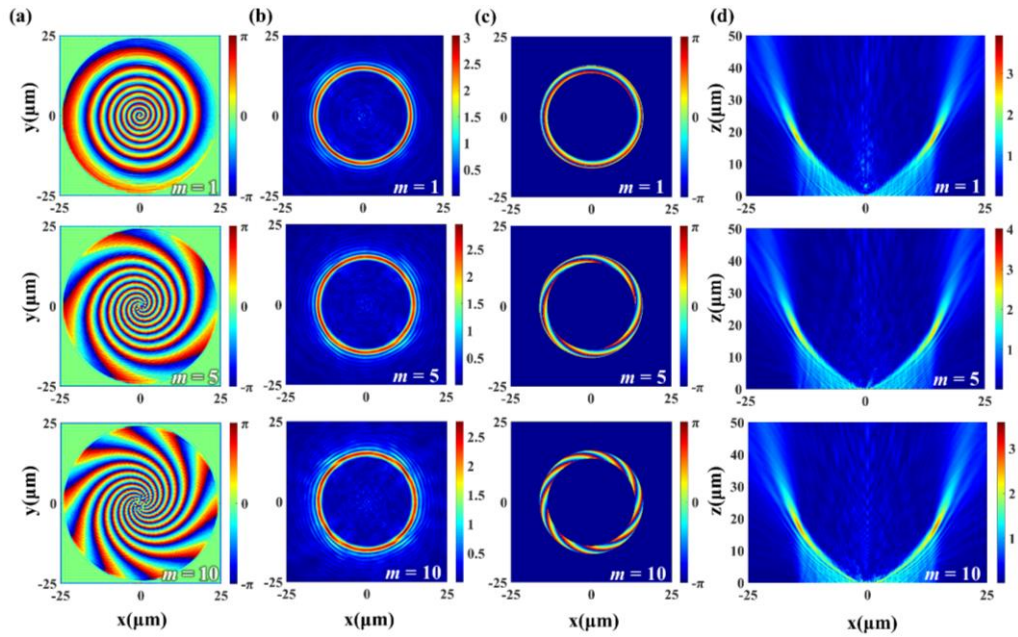


Fig. 4 In the case of axial cone phase divergency, the parameters of the metasurface are $f$ = 20 μm, $\beta$ = 40 °, $m$ = 1, 5, and 10. (a) The phase distributions on the upper surface of the metasurfaces are obtained. (b) Light intensity distributions in the focal plane $z$ = 20 μm. (c) Phase distributions in the focal plane corresponding to the ring-shaped focal spot in the x-y plane. (d) The intensity distribution on the z-transmission plane.

Next, we respectively adjusted $\beta$ and $f$ and observed the influences of these parameters on the light field in the focal plane. Firstly, the influence of the half fan angle $\beta$ of the axicon was considered and it was reduced from 40 ° to 20 ° while the focal length $f$ = 20 μm was maintained. By comparing the solid lines with the dot-dash lines in Fig. 5(a), the radius of the ring-shaped focal spots observed in the focal plane $z$ = 20 μm decreases to about 8 μm with the decrease of $\beta$. Then we studied the effect of focal length $f$ on the PV. We kept $\beta$ = 20 °, increase the designed focal length $f$ from 20 μm to 30 μm. As shown in the dotted lines in Fig. 5(a), the radii of the ring-shaped focal spots in the focal plane of the second group of the PVs were significantly increased, reaching about 12 μm. As shown in Fig. 5(a), three groups of nearly symmetrical distributions of normalized intensity can be obviously observed, which means that in each group of focal planes with different parameters $f$ and $\beta$, the radii of ring-shaped focal spots were basically the same when $m$ changes, which indicated that PVs are generated under all three sets of parameters. Furthermore, we selected the radius of the ring-shaped focal spots in the focal plane under the condition of fixing $m$ = 5 to observe the influence of different parameters $f$ and $\beta$ on the generation of the PV. Fig. 5(b) and (c) illustrate that the radius of the ring-shaped focal spots varies approximately linearly with the change of $f$ or $\beta$. These results indicated that the radius can be controlled in a certain range by designing reasonable parameters $f$ and $\beta$, so as to obtain a more ideal distribution of PVs to meet the needs of different occasions.

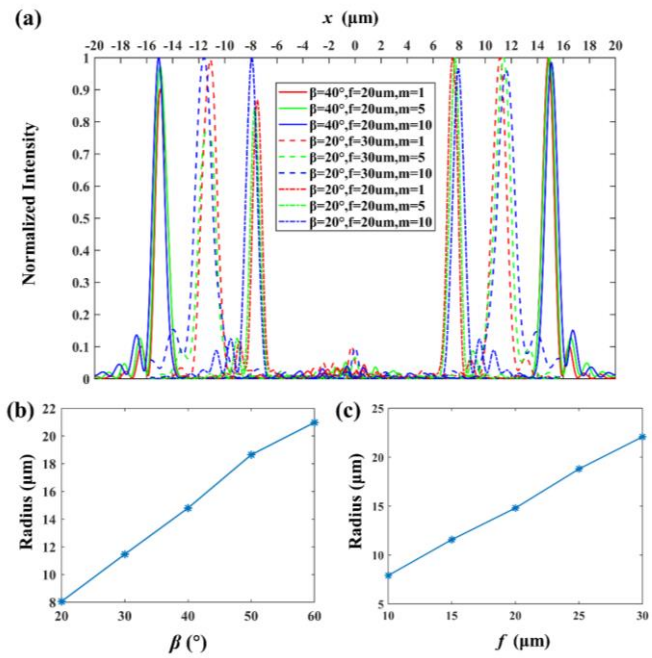


Fig. 5(a) The normalized intensity distributions of $f$ = 20 μm, $\beta$ = 40 ° (solid line); $f$ = 30 μm, $\beta$ = 20 ° (dotted line); $f$ = 20 μm, $\beta$ = 20 ° (dot dash line) at $m$ = 1 (red), 5 (green), and 10 (blue), respectively. (b) Trend of focal plane ring radius with $\beta$ when $m$ = 5, fixed $f$ = 20 μm. (c) Trend of focal plane ring radius with $f$ when $m$ = 5, fixed $\beta$ = 40 °.

However, unlike PB metasurfaces [37, 38, 46], our PV generators have no restrictions on the polarization state of the incident light source. To verify the polarization insensitivity, we performed simulations with four different polarized incidences. The results are displayed in Fig. 6(a), where the maximum positions of the normalized intensities of the PVs in the focal plane remain almost unchanged with different TCs. The ring radius of the generated PVs and the focusing efficiency of PV generators under left-handed circularly polarized, $x$-polarized, and $y$-polarized Gauss incidences are displayed in Table. 1. As the polarization of incidences changes, the results in Table. 1 demonstrate that the radii of PVs with all four kinds of polarized incidences keep consistent and the focusing efficiency of the PV generator is always maintained at a high level. These results fit well with the design, which demonstrate that the metasurface PV generators can

transform the incident Gaussian beam with arbitrary polarization into the PV. In this section, we had successfully generated single focused PVs using polarization-insensitive metasurfaces with the incidence of all four kinds of polarized Gaussian beams and these PV generators also exhibited flexibility in tuning the radii of the generated PVs.

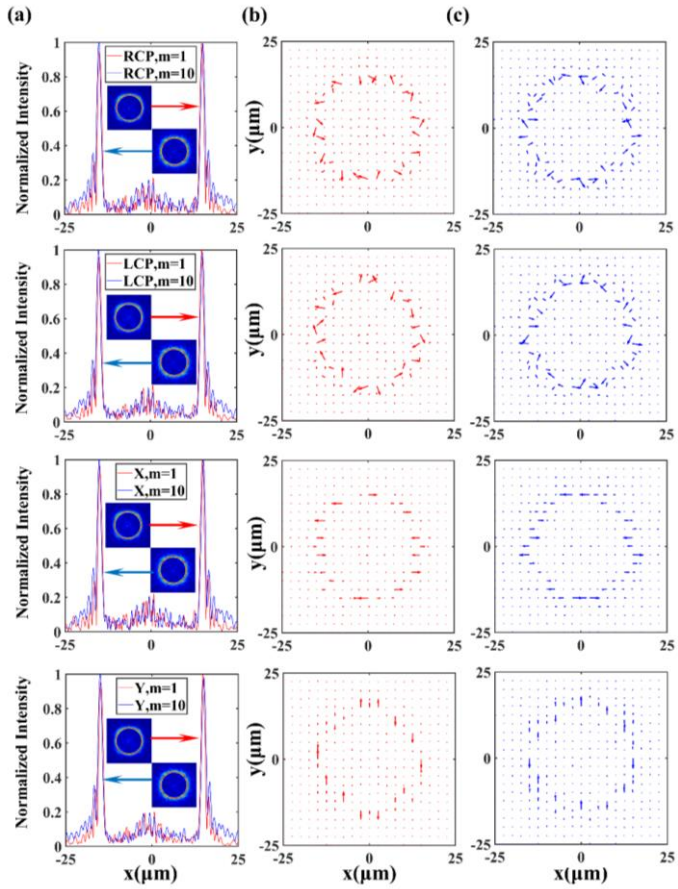


Fig. 6 The parameters of the metasurface are $f$ = 20 μm, $\beta$ = 40°, $m$ = 1 (red), and 10 (blue) with right-handed circularly polarized, left-handed circularly polarized, $x$-polarized, and $y$-polarized incidences, respectively. The arrows in the polarization profile were calculated by $\arctan[\mathrm{Re}(Ey)/\mathrm{Re}(Ex)]$, and the data used here were obtained from the electric field monitor in the focal plane. (a) The normalized intensity distributions in the focal plane with $m$ = 1 and 10. (b) The polarization distribution in the focal plane when $m$ = 1. (c) The polarization distribution in the focal plane when $m$ = 10.

Table 1. The ring radius of PVs and the focusing efficiency of the PV generators with different polarized incidences

| Polarization and TCs | Radius (μm) | Focusing efficiency (%) |
|---|---|---|
| LCP ($m$ = 1) | 14.85 | 67.10 |
| LCP ($m$ = 10) | 15.05 | 63.06 |
| X ($m$ = 1) | 14.90 | 66.74 |
| X ($m$ = 10) | 15.05 | 63.11 |
| Y ($m$ = 1) | 14.85 | 67.83 |
| Y ($m$ = 10) | 15.00 | 63.17 |

*3.2. Multiple PVs*

In the above, single PVs with phase of converging or diverging axicon were generated and we also demonstrated the polarization insensitivity of the PV generators. In optical communication applications, the schemes that generate multiple PVs simultaneously can significantly improve the performance of the system [33, 43-45]. In order to maximize the potential of the monolithic metasurface, we tried two different methods to generate multiple PVs simultaneously. As shown in Fig. 5(b), when $f$ is fixed and only $\beta$ of the axicon is changed, the radii of the ring-shaped focal spots observed in the focal plane are approximately linear with $\beta$. Therefore, we could superimpose four PV phases with different $\beta$ and $m$ on the metasurface under the condition of keeping $f$ unchanged to realize the generation of the coaxial PVs. To achieve the coaxial propagation of multiple PVs, the final phase patterned on the metasurfaces obeys: $\varphi_{\mathrm{sum}} = \arg\left[\sum_{n=1}^{4} \exp\left(i\varphi_{\mathrm{PV},n}\right)\right]$. The phase $\varphi_{\mathrm{PV},n}$ used to generate four individual PVs still obeys Eq. (5). Here, we kept the focal length of the four PVs at $f = 40$ μm and simulated them under two different groups of TCs. The first group is PV1 ($\beta = 15°$, $m = 1$), PV2 ($\beta = 20°$, $m = 3$), PV3 ($\beta = 25°$, $m = 5$), and PV4 ($\beta = 30°$, $m = 7$). The second group is PV1 ($\beta = 15°$, $m = 2$), PV2 ($\beta = 20°$, $m = 4$), PV3 ($\beta = 25°$, $m = 6$), and PV4 ($\beta = 30°$, $m = 8$). As shown in Fig. 7(a), the phase distributions of the metasurface under two groups of parameters are theoretically calculated. And from the center to the external, the simulated phase distributions of the metasurface corresponding PV1 ($\beta = 15°$), PV2 ($\beta = 20°$), PV3 ($\beta = 25°$), PV4 ($\beta = 30°$) were shown in Fig. 7(b). According to Figs. 7(c), four evenly distributed concentric ring-shaped focal spots can be observed on the plane at $z = 40$ μm, with the radius difference of 3 μm between adjacent rings. The change in radii is consistent with the linear expanding trend of the radius of ring-shaped focal spots caused by the increase of $\beta$. In addition, by observing the phase distribution at each ring-shaped focal spot located on the corresponding positions in the focal plane Fig. 7(d), both two sets of PVs with different $\beta$ carry correct TCs and maintain consistent ring radii with different TCs, which means that the ring radius is independent from TCs. That is, simulation results demonstrate that we can realize the coaxial propagation of four PVs through a monolithic metasurface.

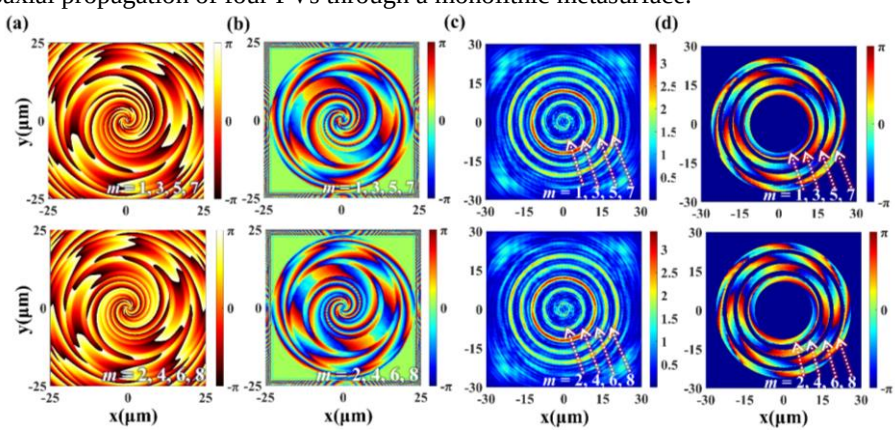


Fig. 7(a) Phase distributions on the metasurface with two sets of parameters are calculated theoretically by *MATLAB*. (b) The phase distributions on the metasurface under the two sets of parameters obtained by simulation (the first set is shown above). (c) Intensity profile from the center to the external corresponding PV1 ($\beta = 15°$), PV2 ($\beta = 20°$), PV3 ($\beta = 25°$), and PV4 ($\beta = 30°$). (d) The phase distributions in the focal plane $z = 40$ μm corresponding to the four ring-shaped focal spots.

Another method to generate multiple PVs simultaneously is to generate multi-channel PVs, which means introducing several PVs with different TCs into linear displacement while keeping $f$ and $\beta$ unchanged and then superimposing their phases on a monolithic metasurface. Here, the phase patterned on the metasurface to

generate multi-channel PVs obeys $\varphi_{\text{sum}} = \arg\left\{\sum_{n=1}^{4}\exp\left[i\left(\varphi_{\text{PV},n} + \left(a_n \cdot x + b_n \cdot y\right)\cdot\frac{2\pi}{A_{xy}}\right)\right]\right\}$, where $A_{xy} = \lambda \cdot f / S_{xy}$, $a_n$ and $b_n$ are parameters that determine the central position of each PV in the focal plane and their value is 0 or ±1. $S_{xy}$ represents the displacement of the centre of each ring-shaped focal spot from the centre of the focal plane in the $x$ or $y$ directions. According to the design, each PV beam propagates at a specific angle away from the $z$-axis, so that four ring-shaped focal spots can be observed at the same time on the focal plane. Here, the four TCs are selected as $m$ =1, 3, 5, and 7, and in order to control the radius of the generated ring to avoid interference between adjacent PVs, we increase the focal length $f$ to 50 μm and restrict the size of each ring by reducing the $\beta$ to 7.5 °, together with the linear displacement factor $S_{xy}$ set as 10 μm. At the focal plane $z = f = 50$ μm, PV1 ($m = 1$, $a_1 = 1$, $b_1 = 0$), PV2 ($m = 3$, $a_2 = 0$, $b_2 = 1$), PV3 ($m = 5$, $a_3 = -1$, $b_3 = 0$), and PV4 ($m = 7$, $a_4 = 0$, $b_4 = -1$) can be simultaneously generated. As shown in Fig. 8(c), the centres of the four rings with almost the same radius in the focal plane are generated at points (0, ±13 μm) and (±13 μm, 0). They are slightly offset from the pre-designed centre position (0, ±10 μm) and (±10 μm, 0). This part of extra offset is probably caused by the metasurface itself. In fact, the actual outgoing light is emitted from the upper surface of each unit cell on the metasurface, while the upper surface of the substrate was set as $z = 0$ μm in the simulation. Because of the designed linear displacement of each PV, when lights reach the design focal plane, the extra offset has been generated. As shown in Fig. 8(d), the stripes corresponding to the designed TC values ($m$ = 1, 3, 5, and 7) also appear at the designed focal point. The simulation results above show that four PVs with different TC values are produced simultaneously at the predetermined position of the focal plane, and there is no overlap between each other.

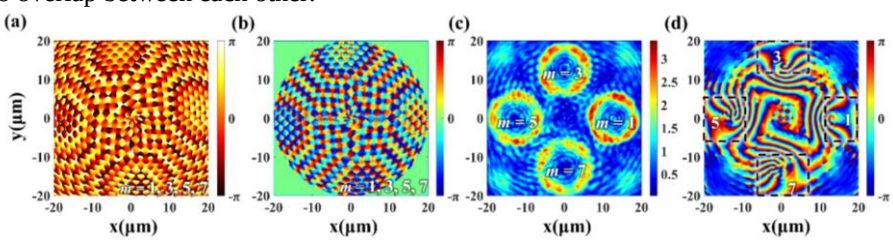


Fig. 8(a) Phase distribution of the upper surface of the metasurfaces calculated theoretically by *MATLAB*. (b) Phase distribution of the upper surface of the metasurfaces obtained by simulation. (c) Diagram of the light intensity distribution in the focal plane, which shows PV1 ($m$ = 1), PV2 ($m$ = 3), PV3 ($m$ = 5), and PV4 ($m$ = 7). (d) Diagram of the phase distribution in the focal plane $z$ = 50 μm.

## 4. Conclusion

In general, by combining the phases of an axicon, a spiral phase plate, and a Fourier transform lens, we designed efficient polarization-insensitive dielectric metasurfaces composed of $TiO_2$ nano-posts with $SiO_2$ substrate to generate PVs. The simulation results indicate that, by designing reasonable parameters $f$ and $\beta$, a more ideal distribution of PVs can be obtained to meet the needs of different occasions, and the polarization-insensitivity to different incidences gives more flexibility for PV generation. In addition, the generation of coaxial PVs and multi-channel PVs through a single metasurface was also successfully achieved by superposing the phase of four PVs with different parameters and introducing linear displacement to PVs with the same $f$ and $\beta$, which can considerably increase the amount of information carried by a single metasurface. The direct generation of PVs by monolithic polarization-insensitive dielectric metasurfaces not only significantly improves the efficiency and flexibility of the optical system, but also greatly improves the integration. Our work will stimulate further applications of PVs in fields such as optical communications, particle manipulation, information storage, and so on, and can supplement the application of metasurfaces in light field control and miniaturized and integrated optical systems.

## Authorship contribution statement

**Zhe Shen:** Conceptualization, Supervision, Writing – review & editing. **Longyin Teng:** Methodology, Formal analysis, Writing – original draft. **Zhiyuan Xiang:** Investigation, Validation. **Le Li:** Writing – original draft. **Yunjie Rui:** Formal analysis. **Yaochun Shen:** Writing - Review & Editing.

## Declaration of Competing Interest

The authors declare that they have no known competing financial interests or personal relationships that could have appeared to influence the work reported in this paper.


## Acknowledgements

This work was supported by National Natural Science Foundation of China (Grant No. 61805119), Natural Science Foundation of Jiangsu Province (Grant No. BK20180469; BK20180468), Fundamental Research Funds for the Central Universities (Grant No. 30919011275).


## Data availability

Data underlying the results presented in this paper are not publicly available at this time but may be obtained from the authors upon reasonable request.

## References


1. L. Allen, M. W. Beijersbergen, R. Spreeuw, and J. P. Woerdman, "Orbital angular momentum of light and transformation of Laguerre Gaussian Laser modes," Phys. Rev. A 45, 8185-8189 (1992).
2. K. T. Gahagan, and G. A. Swartzlander, "Optical vortex trapping of particles," in Summaries of papers presented at the Conference on Lasers and Electro-Optics (1996), pp. 155-156.
3. K. T. Gahagan and G. A. Swartzlander, "Simultaneous trapping of low-index and high-index microparticles observed with an optical-vortex trap," J. Opt. Soc. Am. B 16, 533-537 (1999).
4. V. G. Shvedov, A. S. Desyatnikov, A. V. Rode, Y. V. Izdebskaya, W. Z. Krolikowski, and Y. S. Kivshar, "Optical vortex beams for trapping and transport of particles in air," Appl. Phys. A 100, 327-331 (2010).
5. J. Wang, J. Y. Yang, I. M. Fazal, N. Ahmed, Y. Yan, H. Huang, Y. Ren, Y. Yue, S. Dolinar, and M. Tur, "Terabit free-space data transmission employing orbital angular momentum multiplexing," Nat. Photonics 6, 488-496 (2012).
6. H. Yan, E. Zhang, B. Zhao, and K. Duan, "Free-space propagation of guided optical vortices excited in an annular core fiber," Opt. Express 20, 17904-17915 (2012).
7. S. Li, and J. Wang, "Multi-orbital-angular-momentum multi-ring fiber for high-density space-division multiplexing," IEEE Photon. J. 5, 7101007-7101007 (2013).
8. S. Ramachandran, P. Gregg, P. Kristensen, and S. E. Golowich, "On the scalability of ring fiber designs for OAM multiplexing," Opt. Express 23, 3721-3730 (2015).
9. A. S. Ostrovsky, C. Rickenstorff-Parrao, and V. Arrizón, "Generation of the "perfect" optical vortex using a liquid-crystal spatial light modulator," Opt.s Lett. 38, 534-536 (2013).
10. P. Gregg, P. Kristensen, and S. Ramachandran, "Conservation of orbital angular momentum in air-core optical fibers," Optica 2, 267-270 (2015).
11. J. Ye, Y. Li, Y. Han, D. Deng, Z. Guo, J. Gao, Q. Sun, Y. Liu, and S. Qu, "Excitation and separation of vortex modes in twisted air-core fiber," Opt. Express 24, 8310-8316 (2016).
12. Mingzhou Chen, Michael Mazilu, Yoshihiko Arita, Ewan M. Wright, and Kishan Dholakia, "Dynamics of microparticles trapped in a perfect vortex beam," Opt. Lett. 38, 4919-4922 (2013).
13. M. Z. Chen, M. Mazilu, Y. Arita, E. M. Wright, and K. Dholakia, "Creating and probing of a perfect vortex in situ with an optically trapped particle. " Opt. Rev. 22.1, 162-165 (2015).
14. C. Zhang, C. Min, L. Du, and X. C. Yuan, "Perfect optical vortex enhanced surface plasmon excitation for plasmonic structured illumination microscopy imaging," Appl. Phys. Lett. 108, 780-782 (2016).
15. P. Vaity, and L. Rusch, "Perfect vortex beam: Fourier transformation of a Bessel beam," Opt. Lett. 40, 597-600 (2015).
16. F. Aieta, P. Genevet, M. A. Kats, N. Yu, R. Blanchard, Z. Gaburro, and F. Capasso, "Aberration-free ultra-thin flat lenses and axicons at telecom wavelengths based on plasmonic metasurfaces," Nano Lett. 12, 4932-4936 (2012).
17. N. Yu, P. Genevet, F. Aieta, M. A. Kats, R. Blanchard, G. Aoust, J. P. Tetienne, Z. Gaburro, and F. Capasso, "Flat optics: controlling wavefronts with optical antenna metasurfaces," IEEE J. Sel. Top. Quantum Electron. 19, 4700423-4700423 (2013).
18. Yu, Nanfang, Capasso, and Federico, "Flat optics with designer metasurfaces," Nature Mater. (2014).
19. G. Zheng, H. Mühlenbernd, M. Kenney, G. Li, T. Zentgraf, and S. Zhang, "Metasurface holograms reaching 80% efficiency," Nat. Nanotechnol. 10, 308-312 (2015).

20. C. Pfeiffer, and A. Grbic, "Controlling vector Bessel beams with metasurfaces," Phys. Rev. Appl. 2, 044012 (2014).
21. B. G. Cai, Y. B. Li, W. X. Jiang, Q. Cheng, and T. J. Cui, "Generation of spatial Bessel beams using holographic metasurface," Opt. Express 23, 7593-7601 (2015).
22. Z. Guo, L. Zhu, K. Guo, F. Shen, and Z. Yin, "High-order dielectric metasurfaces for high-efficiency polarization beam splitters and optical vortex generators," Nanoscale Res. Lett. 12, 512 (2017).
23. Z. Lin, X. Li, R. Zhao, X. Song, Y. Wang, and L. Huang, "High-efficiency Bessel beam array generation by Huygens metasurfaces," Nanophotonics 8, 1079-1085 (2019).
24. X. Yi, X. Ling, Z. Zhang, Y. Li, X. Zhou, Y. Liu, S. Chen, H. Luo, and S. Wen, "Generation of cylindrical vector vortex beams by two cascaded metasurfaces," Opt. Express 22, 17207-17215 (2014).
25. Kai, Ou, Guanhai, Li, Tianxin, Hui, Yang, Feilong, Yu, and Jin, "High efficiency focusing vortex generation and detection with polarization-insensitive dielectric metasurfaces," Nanoscale 10, 19154-19161 (2018).
26. F. Ding, Y. Chen, and S. I. Bozhevolnyi, "Focused vortex-beam generation using gap-surface plasmon metasurfaces," Nanophotonics 9, 371-378 (2020).
27. Z. Shen, R. Li, Q. Chen, and B. Zhang, "Numerical study on the tight focusing of radially polarized beams with polarization-insensitive metalenses," J. Opt. 22, 105104 (2020).
28. Y. Liu, Y. Ke, J. Zhou, Y. Liu, H. Luo, S. Wen, and D. Fan, "Generation of perfect vortex and vector beams based on Pancharatnam-Berry phase elements," Sci. Rep. 7, 44096 (2017).
29. M. V. Berry, "Quantal phase factors accompanying Adiabatic changes," Proc. R. Soc. London, Ser. A Math. Phys. Sci. 392, 45-57 (1984).
30. M. V. Berry, "The Adiabatic phase and Pancharatnam's phase for polarized light," J. Mod. Optics 34, 1401-1407 (1987).
31. A. Niv, G. Biener, V. Kleiner, and E. Hasman, "Manipulation of the Pancharatnam phase in vectorial vortices," Opt. Express 14, 4208-4220 (2006).
32. E. Hasman, V. Kleiner, G. Biener, and A. Niv, "Polarization dependent focusing lens by use of quantized Pancharatnam–Berry phase diffractive optics," Appl. Phys. Lett. 82, 328-330 (2003).
33. Y. Zhang, W. Liu, J. Gao, and X. Yang, "Generating focused 3D perfect vortex beams by plasmonic metasurfaces," Adv. Opt. Mater. 6, 1701228 (2018).
34. M. Khorasaninejad, W. T. Chen, R. C. Devlin, J. Oh, A. Y. Zhu, and F. Capasso, "Metalenses at visible wavelengths: Diffraction-limited focusing and subwavelength resolution imaging," Science 352, 1190-1194 (2016).
35. E. Arbabi, A. Arbabi, S. M. Kamali, Y. Horie, and A. Faraon, "Controlling the sign of chromatic dispersion in diffractive optics with dielectric metasurfaces," Optica 4, 625-632 (2017).
36. A. Arbabi, Y. Horie, M. Bagheri, and A. Faraon, "Dielectric metasurfaces for complete control of phase and polarization with subwavelength spatial resolution and high transmission," Nat. Nanotechnol. 10, 937-943 (2015).
37. J. Xie, H. Guo, S. Zhuang, and J. Hu, "Polarization-controllable perfect vortex beam by a dielectric metasurface," Opt. Express 29, 3081-3089 (2021).
38. Q. Zhou, M. Liu, W. Zhu, L. Chen, Y. Ren, H. J. Lezec, Y. Lu, A. Agrawal, and T. Xu, "Generation of perfect vortex beams by dielectric geometric metasurface for visible light," Laser Photonics Rev. 15, 2100390 (2021).
39. A. Arbabi, Y. Horie, A. J. Ball, M. Bagheri, and A. Faraon, "Subwavelength-thick lenses with high numerical apertures and large efficiency based on high-contrast transmitarrays," Nat. Commun. 6, 7069 (2015).
40. E. Arbabi, A. Arbabi, S. M. Kamali, Y. Horie, and A. Faraon, "Multiwavelength polarization-insensitive lenses based on dielectric metasurfaces with meta-molecules," Optica 3, 628-633 (2016).
41. P. Bélanger and M. Rioux, "Ring pattern of a lens–axicon doublet illuminated by a Gaussian beam," Appl. Opt. 17, 1080-1088 (1978).
42. Y. Zhu, D. Wei, Z. Kuang, Q. Wang, Y. Wang, X. Huang, Y. Zhang and M. Xiao, "Broadband variable meta-axicons based on nano-aperture arrays in a metallic film, ", Sci. Rep. 8, 11591 (2018).
43. S. Fu, T. Wang, and C. Gao, "Perfect optical vortex array with controllable diffraction order and topological charge," J. Opt. Soc. Am. A 33, 1836-1842 (2016).
44. F. Yue, D. Wen, C. Zhang, B. D. Gerardot, W. Wang, S. Zhang, and X. Chen, "Multichannel polarization-controllable superpositions of orbital angular momentum states," Advanced materials (Deerfield Beach, Fla.) 29(2017).
45. H. Wang, S. Fu, and C. Gao, "Tailoring a complex perfect optical vortex array with multiple selective degrees of freedom," Opt. Express 29, 10811-10824 (2021).
46. J. He, M. Wan, X. Zhang, S. Yuan, L. Zhang, and J. Wang, "Generating ultraviolet perfect vortex beams using a high-efficiency broadband dielectric metasurface," Opt. Express 30, 4806-4816 (2022)
47. M. Liu, P. Huo, W. Zhu, C. Zhang, S. Zhang, M. Song, S. Zhang, Q. Zhou, L. Chen, H. J. Lezec, A. Agrawal, Y. Lu, and T. Xu, "Broadband generation of perfect Poincaré beams via dielectric spin-multiplexed metasurface," Nat. Commun. 12, 2230 (2021).
48. W. T. Chen, M. Khorasaninejad, A. Y. Zhu, J. Oh, R. C. Devlin, A. Zaidi, and F. Capasso, "Generation of wavelength-independent subwavelength Bessel beams using metasurfaces," Light Sci Appl 6, e16259 (2017).